Robust 3D Reconstruction and Mean-Shift Clustering of Motoneurons from Serial Histological Images

Nicolas Guizard, Pierrick Coupé, Nicolas Stifani, Stefano Stifani, D. Louis Collins

Robust 3D Reconstruction and Mean-Shift Clustering of Motoneurons from Serial Histological Images

Nicolas Guizard[1], Pierrick Coupe[1], Nicolas Stifani[2], Stefano Stifani[2], D. Louis Collins[1]

[1] McConnell Brain Imaging Centre, Montréal Neurological Institute, McGill University, Montréal, Québec, H3A 2B4, Canada
[2] Center for Neuronal Survival, Montréal Neurological Institute, McGill University, Montréal, Québec, H3A 2B4, Canada

Abstract. Motoneurons (MNs) are neuronal cells involved in several central nervous system (CNS) diseases. In order to develop new treatments and therapies, there is a need to understand MN organization and differentiation. Although recently developed embryo mouse models have enabled the investigation of the MN specialization process, more robust and reproducible methods are required to evaluate the topology and structure of the neuron bundles. In this article, we propose a new fully automatic approach to identify MN clusters from stained histological slices. We developed a specific workflow including inter-slice intensity normalization and slice registration for 3D volume reconstruction, which enables the segmentation, mapping and 3D visualization of MN bundles. Such tools will facilitate the understanding of MN organization, differentiation and function.

1 Introduction

Motoneurons (MNs) are neuronal cells from the central nervous system (CNS) whose axons extend outside of the CNS. Several MN diseases, such as amyotrophic lateral sclerosis (ALS), lead to MN cell death correlated with a progressive loss of muscle contractibility. MN specification relies notably on expression of a defined set of transcription factors. Each combination of transcription factors ultimately leads to the formation of a MN pool (or bundle) that shares common characteristics and projects to a common target. Typical amniote limbs are composed of more than 50 different muscles [17], however little is known about the intrinsic identity of the corresponding MN bundles. Recent studies with embryo mouse models, have characterized pool specific transcription factors such as Pea3 [8], Scip and Runx1 [7] providing basic knowledge of MN pool differentiation.
Understanding the mechanisms and the precise topography of the transcription factors underlying MN specification will provide important insights for the elaboration of regenerative therapies (*i.e.* stem cells therapy). In this field, light

microscopy is commonly used to identify MN clusters on 2D embryo mouse slices, with manual identification of the clusters [4]. Usually, an expert identifies the bundle location, the number of MN cells and the cluster diameter on a slice-by-slice basis. However, this process is time consuming and lacks reproducibility when attempting to apply a robust analysis across populations in animal studies. Furthermore, the discontinuity of the 2D histological slices prevents the investigation of the 3D organization of MN clusters. Therefore, there is a need for robust automatic 3D reconstruction, segmentation and clustering.
In this article, we propose a fully automatic approach to MN cluster identification that consists of: inter-slice intensity normalization, reconstruction of corrupted slices, non-linear symmetric inter-slice registration and a 3D Mean-Shift clustering of the MNs.

2 Materials and Methods

2.1 Data Acquisition

Runx1 lacZ/+ mice were generated and genotyped as described in [11]. For embryonic staging, the day of appearance of the vaginal plug was considered as 0.5 embryological day (E0.5). All animal procedures were conducted in accordance with the guidelines of the Council for Animal Care. E13.5 mouse embryos were collected and fixed in 2% paraformaldehyde, 10 mM sodium periodate, and 70 mM l-lysine for 2 hours; transferred to 30% sucrose for 24 hours. After freezing, 14μm cryostat sections were prepared and subjected to immunohistochemistry as described in [11] in order to identify specific MNs. All the resulting slices were captured with an EXi Retiga color camera (QImaging) mounted on an Axio Imager M1 microscope (Zeiss) with a 1.68x1.68μm in-plane resolution (Fig. 1).

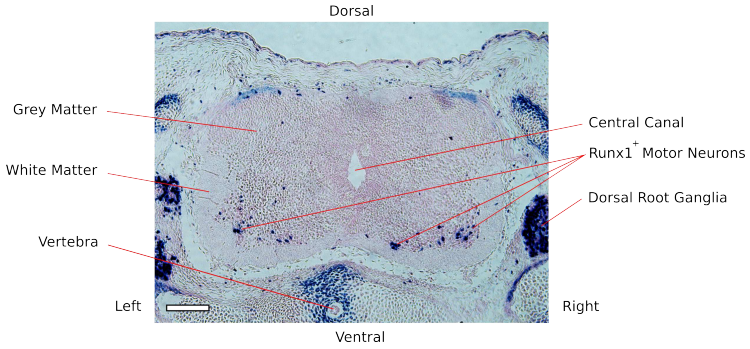

Fig. 1. Example of stained histological embryo spinal slice (scale bar = 40μm) with specific MN staining (blue).

2.2 Workflow

Identification of MN clusters requires segmentation and grouping of MN neurons on each histological slice. While MN neurons are dark and easily segmented, clustering is difficult because: i) intensity differences exist from slice to slice, ii) staining and sectioning may result in lost or corruption of slices (*e.g.* air bubbles, stretching...), and iii) the slices are not aligned within the stack. For each of these limitations we propose an adapted image processing as follows:

Inter-Slice Intensity Normalization Staining inhomogeneity, due in part to local slice thickness variance, can produce intensity inhomogeneities between slices that adversely affect visual analysis and automated registration methods. We used the intensity normalization method proposed by [16] which consists in a linear transformation of the current slice histogram to match the histogram of the reference slice, which in this case is defined as the middle slice of the spinal cord.

Inpainting Cryotomic image acquisition lead to discrepancies such as folding, stretching, splitting as well as air bubbles which can get stuck between the slides. In order to recover the corrupted slices identified during the image acquisition procedure, we applied a robust inpainting method [9]. Initially proposed in magnetic resonance imaging, this approach reconstructs the missing voxels by using the two most similar patches from the previous and the subsequent slices.

3D Image Reconstruction To correct for morphological inconsistencies between the slices due to stretching, distortion, rotation and translation during the slice image acquisition, we propose an iterative 3D reconstruction method based on inter-slice registration as in [10] [5] [6]. While [10] and [5] used a Single Slice (SS) before and after to determine the deformation field, and [6] used a Multi-Slice (MS) reconstruction approach, we proposed a Multi-Slice reconstruction approach based on a symmetric registration non-linear registration and Gaussian-Distance weighted interpolation of deformation field (MSDWsym). The ANIMAL non-linear registration algorithm [2] allows for the registration parameters to be set for histological image dimensions [6]. ANIMAL uses a multi-scale vector deformation estimation with a normalized cross-correlation similarity measure. Local registration is achieved in a hierarchical manner with a Gaussian blurring of input images with kernels of varying size to recover large deformations. To enforce the inter-slice registration consistency and to reduce the effect of outlier slices with erroneous anatomy, the deformation fields T_i (Eq. 1) of the slice i is obtained with a Gaussian distance-weighted average deformation [15] to the 6 nearest slices. This proposed MSDW approach gives a stronger weight to the nearest slices such that:

$$\overline{T}(x)_i = \frac{\sum_{n=-3}^{3} \overline{T}(x)_{i\to n} \exp\left(\frac{n^2}{9}\right)}{\sum_{n=-3}^{3} \exp\left(\frac{n^2}{9}\right)} \tag{1}$$

where $\overline{T}(x)_i$ is the deformation field in x of the image i and n the distance between the reference and the target slices. This iterative process uses the previous iteration deformation field as an initial deformation for the following registration and the iteration number was set to 25. In order to produce less pair-wise registration errors, to avoid registration bias and to preserve the topology of the images [1], we force ANIMAL to be symmetric. To do so, we applied regularization constraints on the forward and the inverse deformation fields [12] for each registration of the MSDW:

$$\overline{T}_{sym}(x)_{i\to j} = \frac{\overline{T}(x)_{i\to j}.(\overline{T}(x)_{j\to i}.\overline{T}(x)_{i\to j}) + (\overline{T}(x)_{j\to i}.(\overline{T}(x)_{i\to j}.\overline{T}(x)_{j\to i}))^{-1}}{2} \tag{2}$$

where $\overline{T}(x)_{i\to j}$ is the deformation field in x of the image i to the image j.

Clustering and localization of the MNs MNs are organized in bundles, with a tubular form along the spinal cord [14]. Due to the slice-by-slice discontinuity, manual outlining of the 2D slices cannot take in consideration the 3D structure of the MNs. A 3D reconstruction step is thus required to realign the structure within a consistent 3D volume to recover the 3D organization of the MNs. Therefore the clustering was performed on the position of the mask-outed MNs extracted from the 3D reconstructed volume using a colour filter. Because the number of MN clusters is still unknown, we applied a spatial Mean-Shift clustering algorithm [13] since it presents the advantage of being a non-a-priori technique. To achieve the Mean-Shift based clusterization, the 2D position $X(x, y)$ of the MNs was used. Moreover, to prevent the loss of continuity between the clusters due to staining and acquisition artefacts that may have omitted MNs, we propose to apply a multi-slice Mean-Shift algorithm. The MN position of the 3 slices before and after are projected into the 2D space of the current slice. The cluster centroids of the current slice are obtained by using all these projected points. This procedure is repeated for each slices of the 3D volume. Since we expect that each cluster is separated by a distance of 30-50μm [4], we set the bandwidth kernel to 40μm. Finally, during the label merging step, the cluster center found in the previous slices is used as a prior to set the label of the next one.

2.3 Experiments

Simulation: We compared 5 different 3D inter-slice reconstruction algorithms: the SS approach [5], MS approach [6] and the proposed approaches with and

without the symmetrization (MSDWsym and MSDW). To validate the 3D reconstruction algorithms, we simulated on 100 identical histological slices stacked together, different random translations, rotations and shearings, which were chosen to mimic acquisition variations (Table 1). The quality of the reconstruction of each method compared was measured by estimating the MN inter-slice overlap with the Dice's Kappa (DK) [3] agreement measure between the ground truth (Fig. 2) and each reconstruction:

$$DK = 2.V(I \cap A)/(I \cup A) \tag{3}$$

where I and A are respectively the initial aligned and automaticly aligned MNs volumes (V). DK value are comprised between 0-1 with 1 indicating perfect agreement. The topology preservation was assessed by comparing the total MN volume difference before and after reconstruction ($|V(I-M)|/V(I)$) where the value closest to 0 the value is the better the topology is preserved.

	Mean	Std	Min	Max
Rotation (°)	0.3	2.8	-4.7	4.9
Translation (μm)	-0.7	4.6	-8.3	8.3
Scale	1.0	0.1	0.87	1.12
Shear	0.0	1.2	-2.0	1.92

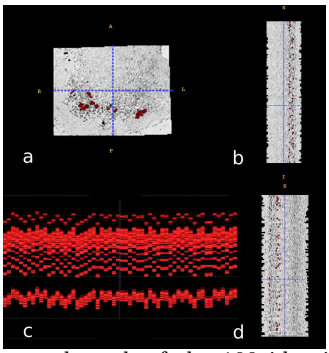

Table 1. Simulation transformation parameters and stack of the 100 identical slice after simulation: axial (a), sagittal (b), coronal (d) and 3D rendering of the MNs(c).

Real data: On a mouse embryo spinal cord data set of 180 slices, we first compared the histogram distance before and after the intensity normalization with the symmetric Kullback-Leibler divergence coefficient (KL). Essentially, small differences between histograms correspond to a lower divergence value. The recent 3D inter-slice reconstruction algorithm of MS [6], our proposed MSDW and MSDWsym methods were evaluated. For both methods, the final results of the clustering was assessed with manual slice-by-slice outlining performed by an expert with a DK agreement measure. The expert performed manual outlining of the clusters on 10 slices in the native space. The automatic clustering of the 10 identical slices after the 3D reconstuction was transformed back in the native space. For each of the methods, the DK agreement measure was compute between the expert and the automatic clustering into the native space.

3 Results and discussion

3.1 Simulation

The 3D reconstructions of the simulated stack obtain by each method are presented in Fig. 2. Visual inspection of the reconstruction shows that the SS reconstruction method resulted in the worst alignment, compared to the multi-slice approaches (MS, MSDW and MSDWsym). Between the multi-slice approaches, MS and MSDW tend to a similar registration quality which seems to misalign the smaller MN clusters present on the top of the images. Because of the regularization, MSDWsym preserves the topology of small structures and provides the best overall registration. Table 2 represents the DK value of the MN mask for the 100 slices after convergence and the percentage of volume preservation. These quantitative results show that MSDWsym reaches higher DK value compared to the MS and MSDW methods. Furthermore the MN volume difference prior to and after reconstruction is best preserved using MSDWsym.

Method	**DK**	% **Volume difference**
SS	0.559	1.9±2.3
MS	0.657	1.4±1.7
MSDW	0.671	1.6±2.1
MSDWsym	0.688	0.4±1.8

Table 2. MN DK overlap measure and topology preservation with MN volume difference prior and after 3D reconstruction.

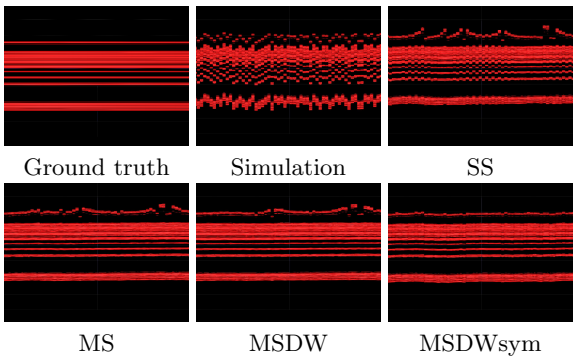

Fig. 2. Sagittal slice of the MN extracted simulated stack.

3.2 Real data

Fig. 3 shows the mouse embryo spinal cord before and after processing. Both sides of the spinal cord are processed separately and the results are visualized together. The slice-to-slice intensity inhomogeneity and mis-registration is visible in the sagittal (c, d) and the coronal (e, f) slices of Fig. 3. After processing, these artefacts are greatly reduced. The average slice-to-slice KL = 0.714 +/- 0.946 before normalization and 0.060 +/- 0.145 afterwards, indicating good agreement of the intensity histograms after normalization. The DK measure (Table 3) between the automatic and the expert segmentation for the different algorithms shows a higher agreement for the MSDWsym 3D reconstruction method. On the axial slices (a, b) of Fig. 3, the inpainting algorithm removed the air bubble but preserved the anatomy of the slide, and most importantly preserved the MN localization and size. Compared to clustering obtained on initial stack (seen in g on Fig. 3), the MN bundles clustering obtained after reconstruction with MSDWsym algorithm (seen in h on Fig. 3) show a continuity and a spacial organization of the MNs.

		DK		
		MS	MSDW	MSDWsym
Cluster	#1	0.622	0.650	0.710
	#2	0.580	0.570	0.700
	#3	0.650	0.670	0.677

Table 3. DK value of expert versus automatic clustering

4 Conclusion and future work

We presented a new approach to investigate MNs differentiation topology in a reproducible and automatic manner. From multiple 2D histological slices of stained mouse embryo spinal cord, we proposed a worklfow to correct for inter-slice intensity inhomogeneity, slice reconstruction, 3D volume reconstruction and MN clustering. We validated our 3D reconstruction method on synthetic data and obtained a better slice-to-slice alignment with the proposed symmetric Multi-Slice Distance-Weighted algorithm (MSDWsym). On real data, the proposed clustering method provides good agreements with the expert manual approach. These results indicate that our method can automatically identify the groups of MNs thank to a sliding Mean-Shift method and a robust 3D reconstruction. Each cluster identified on the left and right side of the spinal cord might target specific limb muscles, and we can also identify sub-clusters that might have more specific targeting. This exploratory study will enable more extensive analyses and validations in the future. In conclusion, the proposed method will facilitate the investigation of different mouse embryo populations and therefore provide important insights for future MN therapies.

References

1. G. E. Christensen and H. J. Johnson. Consistent image registration. *Medical Imaging, IEEE TMI*, 20(7):568–582, 2001.
2. D. L. Collins and A. C. Evans. Animal: Validation and applications of non-linear registration-based segmentation. *IJPRAI*, 11:1271–1294, 1997.
3. Lee R. Dice. Measures of the amount of ecologic association between species. *Ecology*, 26(3):297–302, July 1945.
4. Arber et al. Ets gene er81 controls the formation of functional connections between group ia sensory afferents and motor neurons. *Cell*, 101(5):485–498, May 2000.
5. Chakravarty et al. The creation of a brain atlas for image guided neurosurgery using serial histological data. *NeuroImage*, 30(2):359–376, 2006.
6. Chakravarty et al. Three-dimensional reconstruction of serial histological mouse brain sections. *ISBI, IEEE International Symposium*, pages 987–990, 2008.
7. Dasen et al. A hox regulatory network establishes motor neuron pool identity and target-muscle connectivity. *Cell*, 123(3):477–491, 2005.
8. Livet et al. Ets gene pea3 controls the central position and terminal arborization of specific motor neuron pools. *Neuron*, 35(5):877–892, 2002.
9. Manjón et al. Fetal mri slice reconstruction using 3d inpainting. *NeuroImage*, 47:S72, 2009.
10. Ourselin et al. Reconstructing a 3d structure from serial histological sections. *Image and Vision Computing*, 19(1-2):25–31, 2001.
11. Stifani et al. Suppression of interneuron programs and maintenance of selected spinal motor neuron fates by the transcription factor aml1/runx1. *International Journal of Developmental Neuroscience*, 8:877, 2008.
12. Tao et al. Symmetric inverse consistent nonlinear registration driven by mutual information. *Computer methods and programs in biomedicine*, 95(2):105–115, 2009.
13. K. Fukunaga and L. Hostetler. The estimation of the gradient of a density function, with applications in pattern recognition. *IEEE TMI*, 21(1):32–40, 2003.
14. T. M. Jessell. Neuronal specification in the spinal cord: inductive signals and transcriptional codes. *Nature reviews. Genetics*, 1(1):20–29, 2000.
15. H. Lee and H. Hong. Robust surface registration using a gaussian-weighted distance map in pet-ct brain images. In *Progress in Pattern Recognition, Image Analysis and Applications*, volume 3773, chapter 83, pages 794–803. Springer-Verlag, 2005.
16. L. G. Nyúl and J. K. Udupa. On standardizing the mr image intensity scale. *Magnetic Resonance in Medicine*, 42(6):1072–1081, 1999.
17. G. E. Sullivan. Anatomy and embryology of the wing musculature of the domestic fowl (gallus). *Australian Journal of Zoology*, 10(3):458+, 1962.

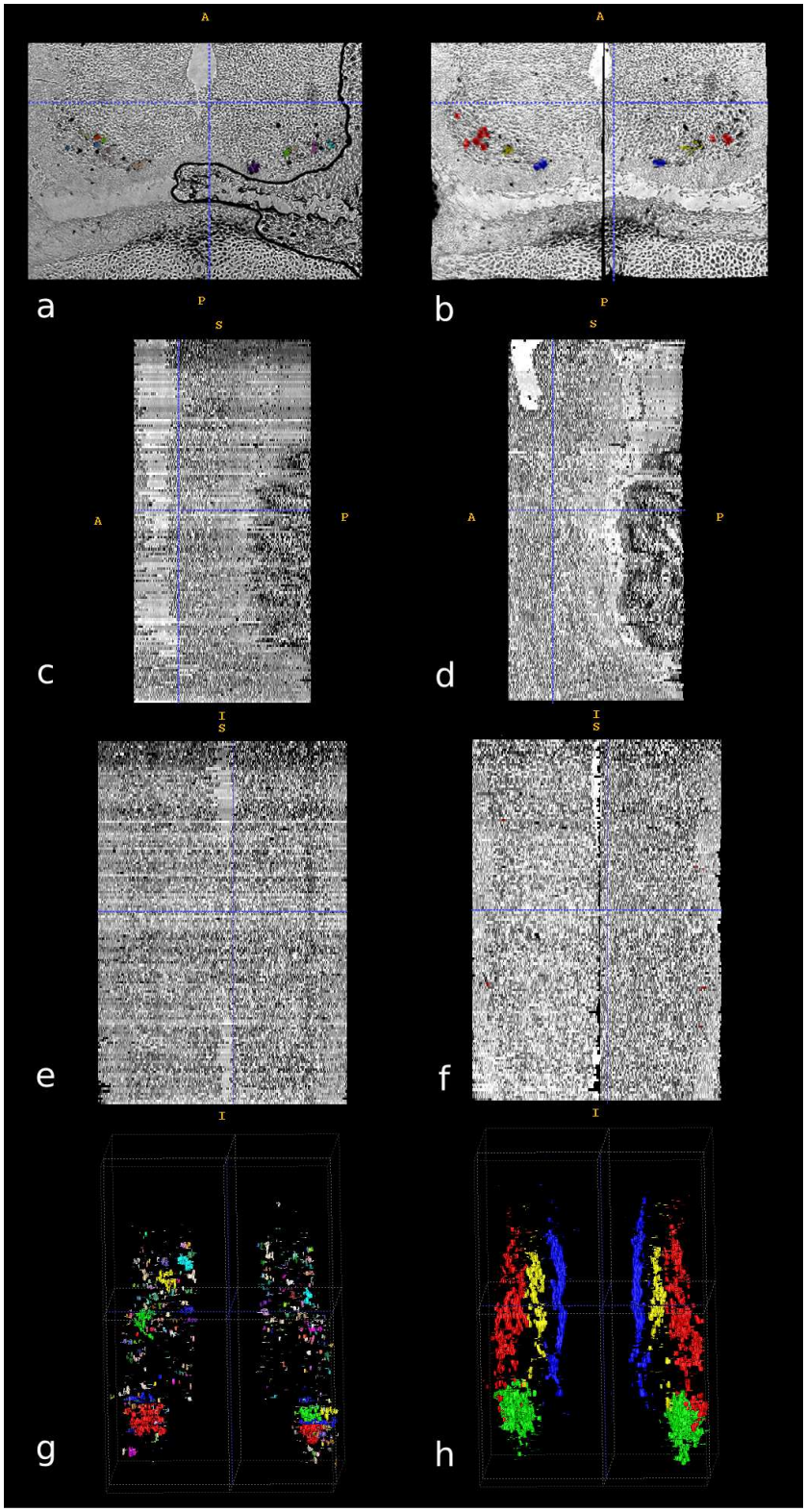

Fig. 3. MN clustering before (a,c,e,g) after (b,d,f,h) 3D reconstruction: axial (a, b), sagittal (c, d), coronal (e, f) and 3D rendering of the MN clusters (g, h).